Effective Use of MSC/NASTRAN Parabolic Tetrahedral Elements

B. William Rudd
David Tompkins
SDRC CAE International
Milford, Ohio

Introduction

Tetrahedral elements have traditionally had little use for a number of reasons:

— The linear tetrahedron is clearly too stiff for practical structural analysis applications.

— Traditional mesh generators can not easily generate the elements.

— More tetrahedral elements are required to model a given geometric region than hexahedra, and each node typically has more tetrahedral elements attached to it (hence increasing analysis time).

— There are no natural planes of nodes within a tetrahedral model. This makes it difficult to perform certain checks and to review the analysis results.

In spite of the limitations, modern free mesh generation techniques that can generate models with tetrahedral elements very quickly for complex geometries have brought renewed interest in using these elements. There are certainly modeling advantages, but most users are concerned about the analysis results. Since the linear tetrahedron element has a bad reputation, users are understandably wary of using the new parabolic tetrahedron element.

MSC has added a parabolic tetrahedron element to NASTRAN. Although this element has given excellent results, there is a relatively small base of experience. SDRC has had good success in applying it in structural and heat transfer applications, and some of these experiences are documented here.

Free Mesh Generation

The primary reason there is interest in a tetrahedron element is due to certain modeling advantages. Dividing an arbitrary solid geometric region into hexahedra in an automated fashion is not as easy to perform as dividing the region into tetrahedra. While there are commercial products that can deal with the tetrahedral subdivision, there are none that handle the hexahedral subdivision in a totally automated fashion. To obtain a hexahedron mesh the user is normally required to spend significant time breaking the model into five or six faced geometric regions that the mesh generator can typically handle. The more automated the mesh generator, the less time required to create the finite element model.

Element Checks

One of the difficulties that arises when building finite element models with tetrahedra is the checking process. There are no natural planes of nodes as in a hexahedra model, thus making it difficult to visualize the entire model. The user must rely on automated checks to have confidence that the model generated is as intended. Hidden line displays can help with the visualization, but more checks are necessary. One method of checking element distortion that is fairly common is a Jacobian check. The program checks the Jacobian determinant at all of the integration points in the element and reports the smallest value (typically after it is normalized) [1]. This gives a feel for the quality of the mapping to the parent element. For a hexahedron, this number will reflect problems such as warped faces, skewed elements, and midnode position. However, performing this check for the tetrahedron element will only reflect the midnode position. As an element deviates from the parent element, the Jacobian values do not change (as long as midnodes are at the midpoint locations). This means that a normalized Jacobian determinant would report a perfect value of 1. until the element's volume is 0. (all four corner nodes in the same plane), at which time the determinant of the Jacobian would be equal to 0.

The user would typically like to know the relative distortion of an element, not just whether it is totally collapsed. To accomplish this, another scheme known as the stretch parameter was developed. The stretch parameter is calculated by inscribing a sphere inside of the tetrahedron (assuming straight edges), and taking the ratio between the radius of this sphere and the longest edge. This value is normalized using the ratio for an equilateral tetrahedron. As an element occupies less and less volume, the stretch parameter will decrease, giving the user a feel for the change in element shape.

Beam Results

In order to compare the behavior of tetrahedron elements with hexahedra, several different cantilever beam models were created using each element type, and MSC/NASTRAN runs were made. The goal was to compare the results from identical models using the two element types. The beam dimensions (10 units long by 1.5 deep by 2 high) created a relatively short beam where shear effects could have an influence. The other properties were set as follows: $E = 1.5E6$, $\upsilon = .29$, $\rho = .0617981$.

A total of eight different models were used. Three models were made of parabolic hexahedron elements. Each of these was used to create parabolic tetrahedron models. Each hex element was broken into five tetrahedra. A single element example showing this breakdown is in figure 1.

The first model consisted of four CHEXA elements (figure 2). A parabolic tetrahedron model (model 2) was created from model 1 (figure 3). The next model (model 3) was also created using four CHEXA elements, but the internal faces were slightly angled (figure 4). Most real life models can not be created using parallelepipeds, and result in angled or warped faces. Figure 5 shows the corresponding tetrahedron model (model 4). Model 5 (figure 6) contained 8 hexahedron elements, while model 6 (figure 7) is the corresponding tetrahedron model.

The next model (model 7) was a tetrahedron model generated from a hexahedron model, but the corresponding hexahedron model was not used. The intention of this model (shown in figure 8) was to create tetrahedrons with a small stretch parameter. This results in a model with a much larger number of elements.

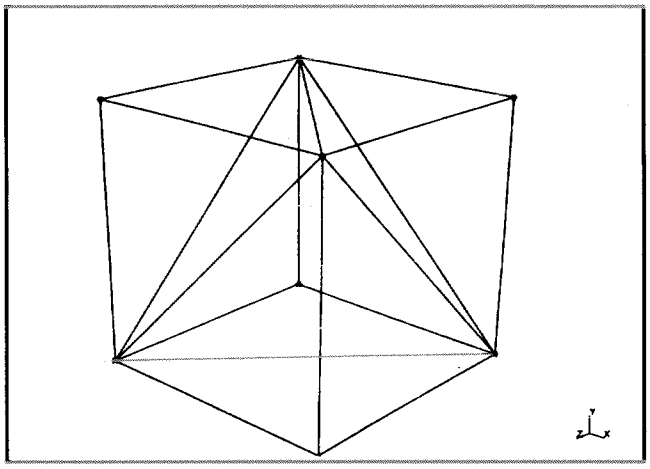

Figure 1. Five Tetrahedra in One Hexahedron.

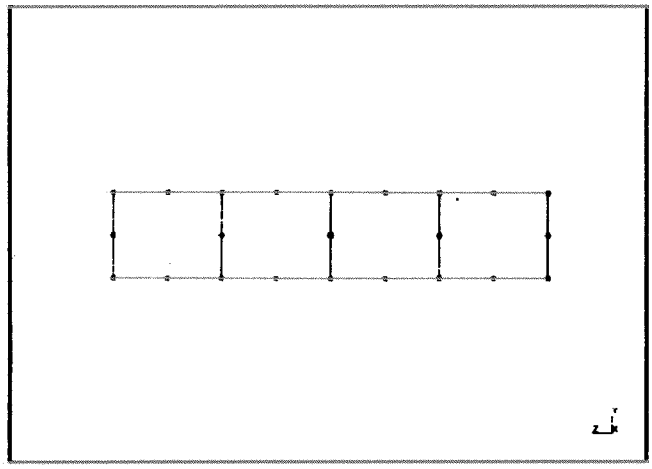

Figure 2. Model 1—Four Hexahedra.

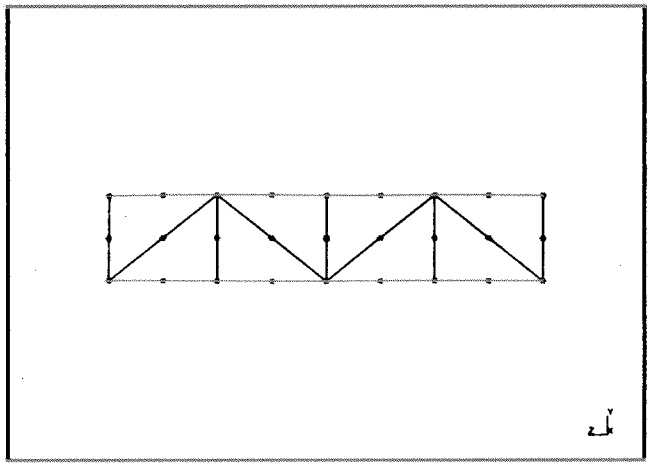

Figure 3. Model 2—Tetrahedra from Model 1.

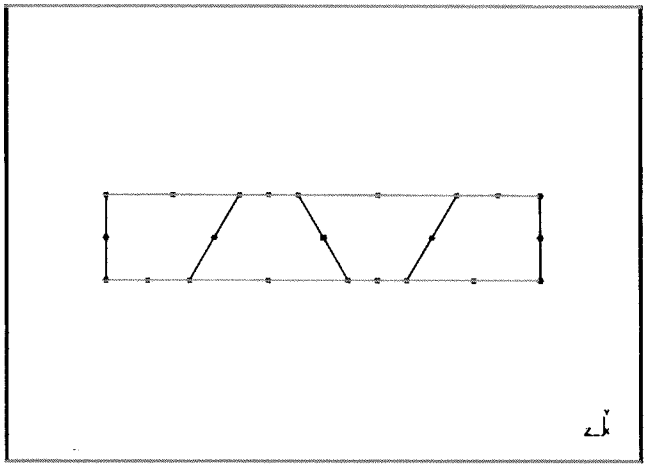

Figure 4. Model 3—Distorted Hexahedra.

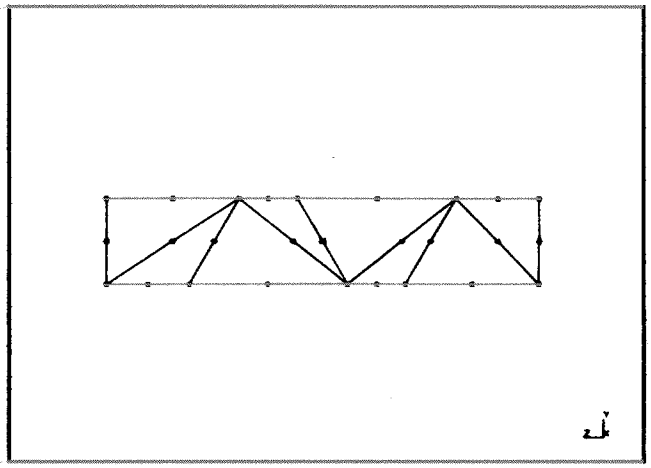

Figure 5. Model 4—Tetrahedra from Model 3.

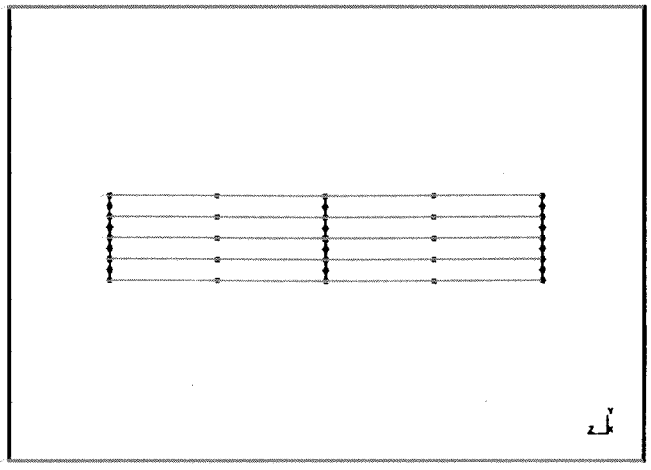

Figure 6. Model 5—Eight Hexahedra.

The final model (model 8) is also a tetrahedron model. These elements were created using the free mesh generator within I-DEAS™ Supertab®. The models generated in this fashion are not generally as ordered as those created by breaking apart hexahedrons. Figure 9 shows that this is the case.

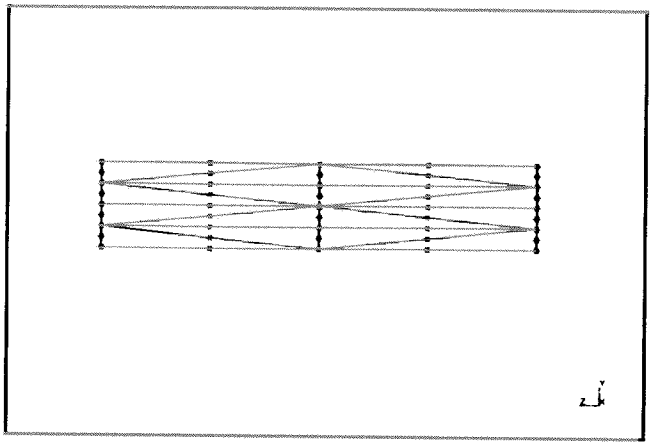

Figure 7. Model 6—Tetrahedra from Model 5.

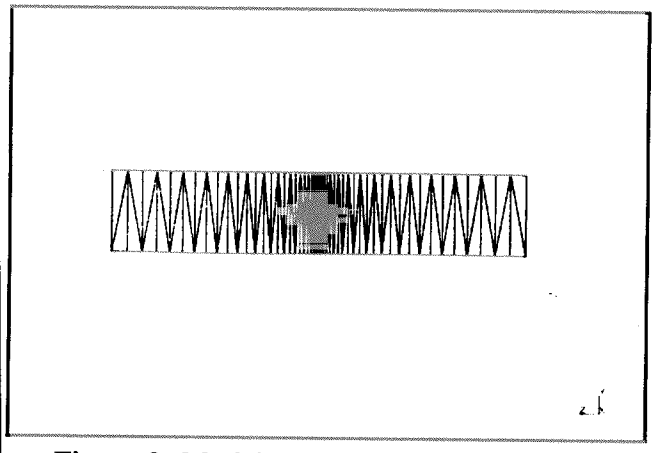

Figure 8. Model 7—Distorted Tetrahedra.

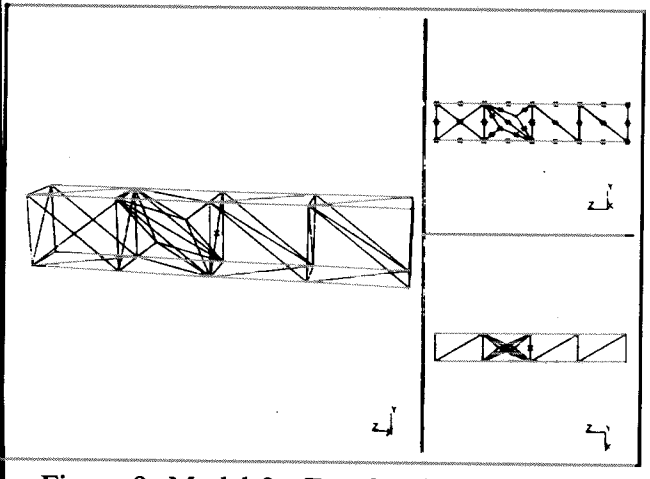

Figure 9. Model 8—Free Mesh Tetrahedra.

Table 1 contains some model information. The distortion range uses the stretch parameter for the tetrahedron and the minimum Jacobian for the hexahedron.

The first load case applied was a pure bending moment. Shear effects did not enter the problem, and the correct answer could be determined using standard beam equations [2,3].

$$V = \frac{MX^2}{2EI} \qquad V = \frac{3E4 \bullet 10^2}{2 \bullet 1.5E6 \bullet 1} = 1.$$

$$u = \frac{1}{2}\int_0^L \left(\frac{M^2}{EI}\right) dx \qquad u = \frac{1}{2}\int_0^{10} \frac{(3E4)^2}{1.5E6 \bullet 1} dx = 3000.$$

The results are presented in Table 2. The theoretical solution for the displacement is a second order polynomial. When the shape functions are complete second order polynomials, the results calculated should be exact. Model number 3, the distorted hexahedron model, is the only model that does not produce exact answers. This is due to the fact that the shape functions for a hexahedron element are complete second order polynomials only if the element is a parallelepiped. By comparison, the tetrahedron model produces exact results for each model, even when the elements become squashed.

The second load case was a shear load. The beam equations used for this problem do not take into account the shear effects.

$$V = \frac{Fx^2}{6EI}(x - 3L) \qquad V = \frac{4500 \bullet 10^2}{6 \bullet 1.5E6 \bullet 1}(10 - 3.10) = -1.$$

$$u_b = \frac{1}{2EI}\int_0^L F^2 x^2 \, dx \qquad u_b = \frac{1}{2 \bullet 1.5E6 \bullet 1}\int_0^{10} 4500^2 \bullet 10^2 dx = 2.25E3$$

The additional strain energy due to shear can be calculated using the following equation.

$$u_s = \frac{1}{2G}\int \tau^2 \, dv \qquad u_s = \frac{9}{15}\frac{F^2 L}{G\,bh}$$

$$u_s = \frac{9}{(15 \bullet 5.814E5)}\frac{4500^2 \bullet 10}{1.5 \bullet 2} = 69.6$$

$$u_T = u_b + u_s = 2.25E3 + 69.6 = 2.3196E3$$

The displacement used for comparison in Table 3 was calculated using a detailed finite element model. This displacement was calculated as 1.019 instead of 1.000. All of the models correlated fairly well, and the hexahedron models tended to be stiffer than the corresponding tetrahedron models. The final area examined was the frequency and shape of the first bending mode. These runs were made using the modified Givens eigensolution. The ASETs for each problem were similar. Degrees of freedom were used only in the direction of the bending mode desired. Figure 10 shows the ASET used for the first problem. Once again, the shear effects enter the problem. Beam theory gives the equations as follows [4].

$$\omega = \frac{1.875^2}{L^2}\sqrt{\frac{EI}{\rho A}} \qquad \omega = \frac{1.875^2}{10^2}\sqrt{\frac{1.5E6 \bullet 1}{.061798096 \bullet 3}} = 100.$$

$$y = .5\left[\left(\cos 1.875\frac{x}{L} - \cosh 1.875\frac{x}{L}\right)\right.$$

$$\left. -.7341\left(\sin 1.875\frac{x}{L} - \sinh 1.875\frac{x}{L}\right)\right]$$

The detailed finite element model used for the shear problem was also used to calculate the frequency for the first bending mode. This value was 97.79, compared to a value of 100. using the beam equations. Figures 11 and 12 show a comparison between the calculated mode shape and the correct (beam) mode shape, for models 1 and 2. Once again, all the models correlate fairly well.

The tetrahedron models provide results that are comparable to the hexahedron models in each of the cases. It would be worthwhile to create a model that is much longer than the model that was used in order to reduce the shear effects in the shear load case and the dynamic calculation. By doing this, it might be possible to draw additional conclusions.

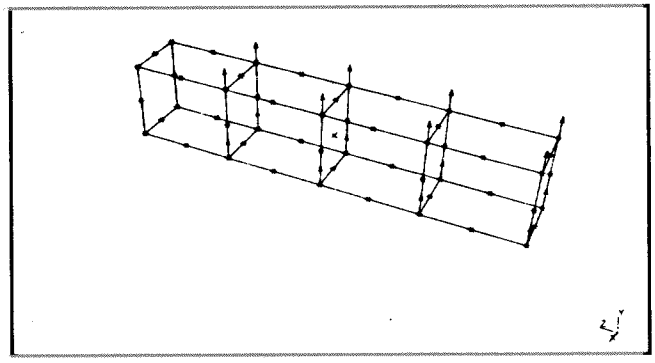

Figure 10. Model 1
with 16 ASET Degrees of Freedom

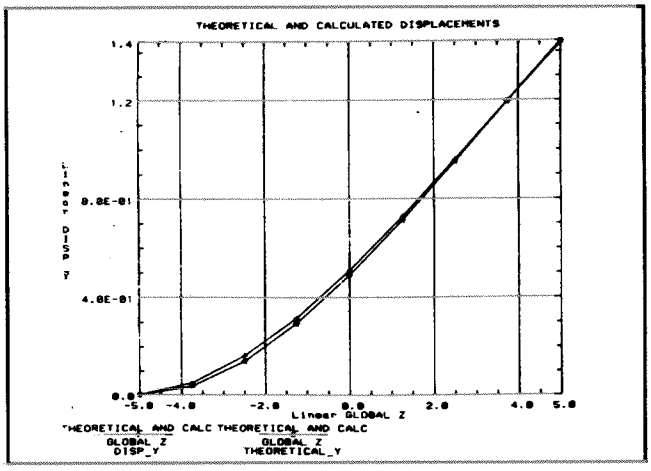

Figure 11. Model 1 Mode Shape Comparison
(Calculated vs. Theoretical)

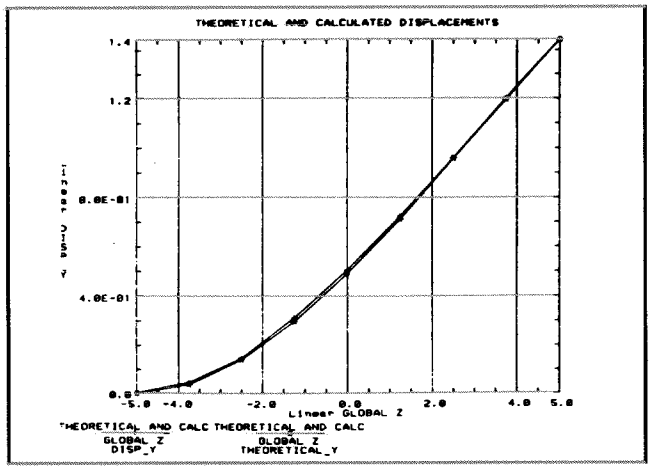

Figure 12. Model 2 Mode Shape Comparison
(Calculated vs. Theoretical)

Table 1—Model Information

No.	Model Description	Number of nodes	Number of elements	Distortion Range	Bandwidth MAX/RMS
1.	4 Hexa	56	4	$1.0 < D < 1.0$	20/13
2.	4 Tetra	77	20	$.61 < D < .83$	24/14
3.	4 Dist Hexa	56	4	$.64 < D < .82$	20/13
4.	4 Dist Tetra	77	20	$.45 < D < .81$	24/14
5.	8 Hexa	89	8	$1.0 < D < 1.0$	29/19
6.	8 Tetra	127	40	$.19 < D < .22$	40/24
7.	Bias Tetra	859	250	$.05 < D < .37$	27/15
8.	Free Tetra	95	34	$.28 < D < .67$	32/17

Table 2—Results for Bending

No.	Model Description	Correct = 1.0000000 Displacement	% Error	Correct = 3000.0000 Strain Energy	% Error
1.	4 Hexa	.999999	0. %	2999.9998	0. %
2.	4 Tetra	.999999	0. %	2999.9998	0. %
3.	4 Dist Hexa	.9915310	-.847%	2975.4402	-.82%
4.	4 Dist Tetra	.999999	0. %	2999.9998	0. %
5.	8 Hexa	.999999	0. %	2999.9999	0. %
6.	8 Tetra	.999999	0. %	2999.9998	0. %
7.	Bias Tetra	.999998	0. %	2999.9998	0. %
8.	Free Tetra	.999998	0. %	2999.9995	0. %

Table 3—Results for Shear

No.	Model Description	Correct = 1.019 Displacement	% Error	Correct = 2319.6 Strain Energy	% Error
1.	4 Hexa	1.034	1.47 %	2326.7	.30 %
2.	4 Tetra	1.022	.33 %	2302.3	-.75 %
3.	4 Dist Hexa	1.019	.01 %	2290.6	-1.25 %
4.	4 Dist Tetra	1.016	-.27 %	2287.4	-1.39 %
5.	8 Hexa	1.035	1.57 %	2329.8	.44 %
6.	8 Tetra	1.004	-1.43 %	2263.6	-2.41 %
7.	Bias Tetra	1.039	1.93 %	2336.1	.71 %
8.	Free Tetra	1.024	.50 %	2305.6	-.60 %

Table 4—Dynamic Results for First Bending Mode

No.	Model Description	Correct = 97.79 Frequency	% Error
1.	4 Hexa	96.79	-1.02 %
2.	4 Tetra	97.68	-.11 %
3.	4 Dist Hexa	97.82	.03 %
4.	4 Dist Tetra	98.16	.38 %
5.	8 Hexa	96.83	-.98 %
6.	8 Tetra	99.53	1.78 %
7.	Bias Tetra	96.52	-1.30%
8.	Free Tetra	97.48	-.32 %

Results Review

When the analysis is complete and the user wishes to examine results, another problem arises. The irregular shapes and numbering make it more difficult to reference a listing. In order to examine results it is generally necessary to rely more on a post processor that can display results graphically.

Figures 13 through 15 show contour plots made using I-DEAS. These plots were made using arbitrary cutting planes through one of the tetrahedron models at an arbitrary location (as shown in the figures). The contour plot is created by interpreting the nodal values that are on the elements cut by the user-defined cutting plane. Note that there is no requirement for nodes on the model to lie on the cutting plane. Cutting planes can also be used to create deformed geometry plots. They are particularly helpful with tetrahedron elements because of the irregular shape, but they can be generated for other types of elements as well.

Applications

The applications of this modeling technique to specific solid components, including a diesel engine piston and a component of a crawler tractor undercarriage (track link) were investigated. Each represented a different class of structure, having unique characteristics. The diesel engine piston represented a "walled" casting while the track link was a solid forging.

Piston—A quarter-sector geometric model of a diesel engine piston was developed using I-DEAS Geomod®. The geometry was then transferred to the free mesh generator in I-DEAS Supertab and a mesh of parabolic tetrahedron finite elements was generated. The resulting finite element model is shown in figure 16. A significant time saving was realized using this modeling approach, and was estimated to be between 50% and 60% over conventional methods. A 4-5 week task was reduced to a 2-3 week task. The quality of the resulting model was determined by performing a MSC/NASTRAN analysis, and comparing results to those from an earlier analysis using hexahedron elements and a more conventional modeling approach. The following loading conditions were considered:

— mechanical load (gas pressure)

— thermal load

Elemental pressures were applied to simulate the gas pressure load. These elemental pressures were actually applied to membrane shell elements which were included on all pressurized surfaces of the piston. Stress data was interrogated using color stress contour plots, which were based upon averaged tetrahedron nodal data. Correlation with the hexahedron model results was very good.

Several heat transfer test cases were performed using both linear and parabolic tetrahedrons. In these tests the linear element actually gave more accurate answers than the parabolic element. This may have been due in part to the lack of a parabolic triangle heat boundary element. After performing these test cases, it was decided to convert the parabolic tetrahedron model to a linear tetrahedron model in order to perform the heat transfer analysis. Convective heat boundary elements were added to the model, film coefficients and bulk temperatures were specified, and a MSC/NASTRAN analysis was performed. Again, correlation with the hexahedron model was very good.

Temperatures from the heat transfer analysis were used as input for the thermal load analysis. Resulting corner node temperatures were averaged to define midnode temperatures along a given edge of the parabolic model. Membrane shell elements covered all free surfaces of the parabolic tetrahedron model, and were the source of the stress data presented. Stress data was interrogated using stress criterion plots, which were based upon unaveraged elemental data.

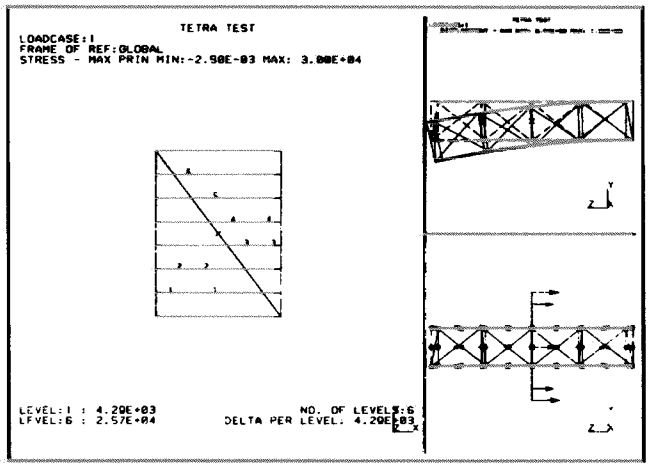

Figure 13. Model 1 with Contours on Cutting Plane (Location 1)

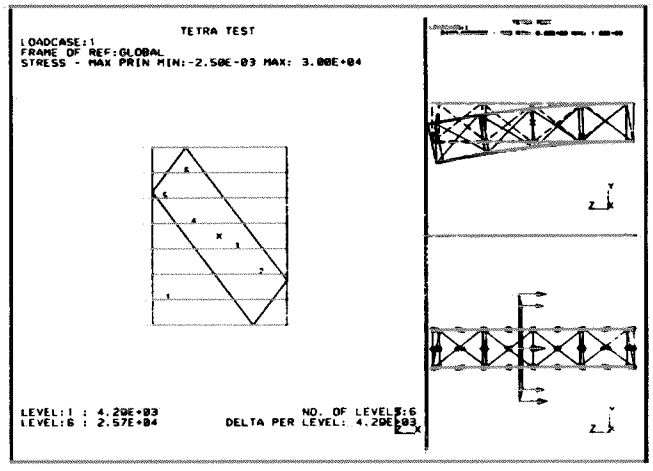

Figure 14. Model 1 with Contours on Cutting Plane (Location 2)

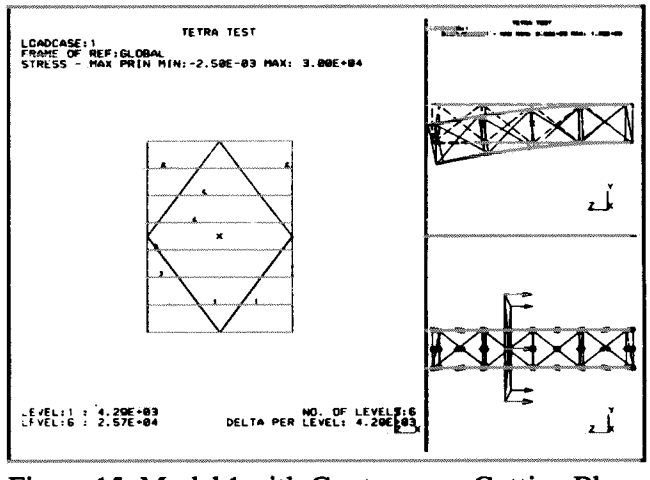

Figure 15. Model 1 with Contours on Cutting Plane (Location 3)

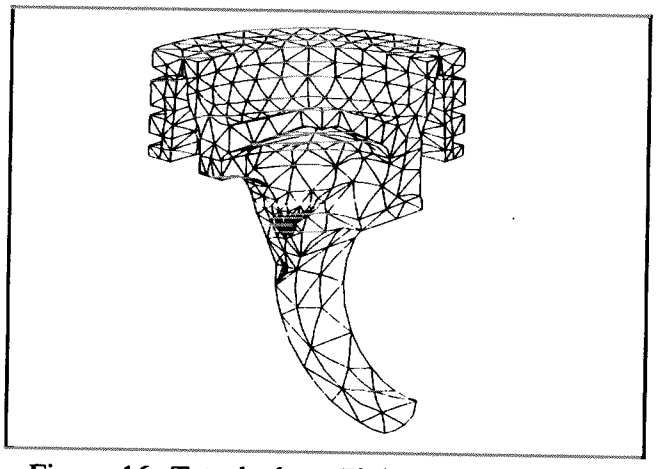

Figure 16. Tetrahedron Finite Element Model of Piston.

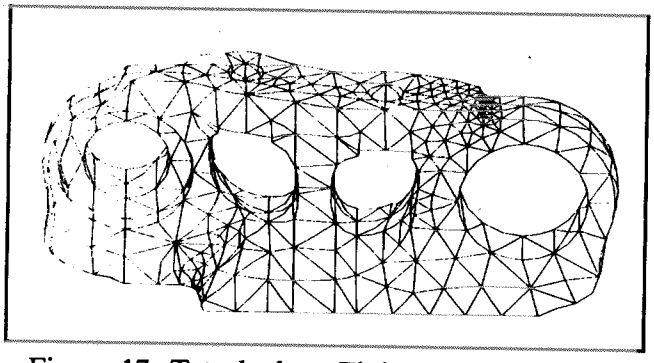

Figure 17. Tetrahedron Finite Element Model of Track Link.

A single parabolic membrane shell element covering the free surface of a parabolic tetrahedron element proved to be inadequate, however. The use of four linear membrane shell elements per face resulted in much better correlation with the hexahedron model stress data. This improved correlation was attributed to the availability of four independent stress tensors from four linear membrane elements, as opposed to three independent stress tensors from one parabolic membrane element. A refined mesh of parabolic tetrahedron elements with parabolic membrane shell elements would be expected to yield comparable results. This would be a more costly alternative, and the refined mesh density was not required to produce acceptable results for other loading conditions. An overall comparison showed that the tetrahedron model results agreed within 5% of the baseline hexahedron model results, considering all loading conditions. The results summary is shown in Table 5 [5].

Table 5—Piston Results

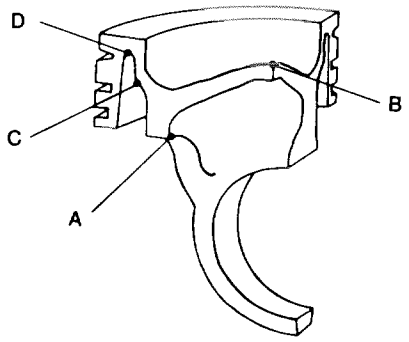

	% Deviation—Tetrahedron Model vs. Hexahedron Model
Mechanical Load —Location A	−4.4% (Principal Stress)
Heat Transfer —Location B	+0.3% (Temperature)
Thermal Load —Location C —Location D	+2.2% (Principal Stress) −1.7% (Principal Stress)

Track Link—A geometric model of a track link was also created with I-DEAS Geomod and used to generate a parabolic tetrahedron finite element model, as shown in figure 17. Again, a time savings in excess of 50% was attained over the conventional solid finite element modeling approach. A 6-7 week task was reduced to a 3-4 week task. The quality of this model was also assessed by performing a MSC/NASTRAN analysis and comparing results to those obtained with a hexahedron model. The hexahedron model results had previously been favorably compared with test results. Two mechanical loading conditions were considered:

— Link tension load.

— Link torsion load.

In each case, the loads were applied as nodal forces. Stress data were interrogated using color stress contour plots, which were based upon averaged tetrahedron nodal data. The peak stress areas identified compared well with those identified by the conventional analysis although some deviation in magnitude was observed. The deviation was within 10%, and was attributed to insufficient element density in the tetrahedron finite element model. A summary of results is presented in Table 6 [5].

Table 6—Track Link Results

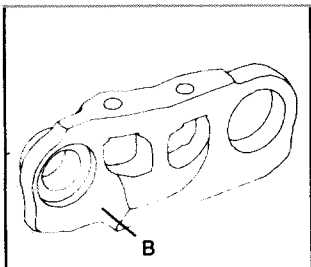

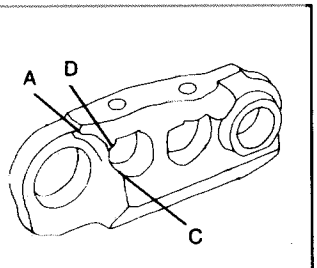

	% Deviation—Tetrahedron Model vs. Hexahedron Model
Link Tension Load	
—Location A	−2.1% (Principal Stress)
—Location B	+12.2% (Principal Stress)
Link Torsion Load	
—Location A	−2.1% (Principal Stress)
—Location C	+8.4% (Principal Stress)
—Location D	+9.2% (Principal Stress)

Conclusions

Although the parabolic tetrahedron finite element is relatively new, it shows great potential for helping to reduce the overall timeframe of building finite element models and reviewing results. This time savings can be greater than 50% for many types of problems. Results have been compared on both theoretical and practical problems without any significant difference in performance.

While analysis run times may be longer, the free mesh generation techniques that create the tetrahedron saves time, and cuts down on user interaction required to set up the meshing process. Analyses like those covered in this paper are being performed on a day to day basis. The results obtained using tetrahedra tend to agree quite well with the results obtained using hexahedra. What is needed to use the tetrahedron confidently is a base of experience, and this experience can only be gained by building real life models as well as performing test cases. More is being learned continually, but the benefits are great enough to warrant using the tetrahedron today.

References

1. Segerlind, Larry J.; Applied Finite Element Analysis; John Wiley & Sons; New York, New York; 1984
2. Roark, Ronald J.; Young, Warren C.; Formulas for Stress and Strain, Fifth Edition; McGraw-Hill Company; New York, New York; 1975
3. Hoff, Nicholas John; The Analysis of Structures; John Wiley & Sons, Inc.; New York, New York; 1956
4. Harris, Cyril M.; Crede, Charles E.; Shock & Vibration Handbook, Second Edition; McGraw-Hill, Inc.; 1976
5. Millburg, Mark; Bedford, Bill; Olson, Doug; "Reducing the Timeframe of Analytical Simulations Using Geometric Modeling and Mesh Generation"; International Off-Highway & Powerplant Congress & Exposition; Milwaukee, Wisconsin; September 8-11, 1986

Acknowledgement

Thanks to Michael Welch and James Poindexter for their assistance in compiling the results of the various beam problems.